Research Paper   Open Access

AI Learning and Characterization of the Printability of Aloe Gel Polysaccharide-Based Alternative Food Ink for 3D Food Printing

Dong-Myong Kim[1,2*,] Hyung-Kon Lee[1], Yong-Seong Kwon[1,2], Yeon-Mea Choi[2], Greethi Lavi[3], Abdul Kahid[3], Dae-Hyun Kim[3]

[1]R&D Center of KJMbio Co. Ltd, Seoul, Korea
[2]KimJeongMoon Aloe Ltd., Seoul, Korea
[3]Nano Process & Device Laboratory of Hanyang University,Seoul, Korea
[*]Corresponding Author

ABSTRACT :*Recently, there has been increasing demand and interest in 3D food printing for manufacturing alternative foods and nanofoods, predicting the printability of food-grade materials as alternative foods based on their biopolymer composition and rheological properties is an important task. This study developed two imagery-based printability assessment metrics: printed filaments' width and roughness and used these metrics to evaluate the printability of Aloe gel-based food inks using response surface methodology (RSM) with regression analysis and machine learning. Aloe gel polysaccharide-based 3D food printing ink is formulated to successfully dispense with Print2taste Mycusini inkjet printers. The polymer ink was then sprayed onto amorphous cellulose powder to observe the powder-binder interaction. Material combinations and parameters were optimized to create a cohesive geometry. Here, the rheological and compositional properties of alternative food-grade inks prepared using Aloe gel pectin (AGP) and Aloe gel cellulose nanoparticle (AGCN) with different ionic cross-linking densities were used as predictors of printability. RSM and linear regression showed good predictability for rheological properties based on formulation parameters, but were unable to predict printability indices. For the machine learning-based prediction model, printability metrics were binarized to pre-specified thresholds and a random forest classifier was trained to predict the overall printability of the ink as well as the filament width and roughness labels using equations and rheological parameters. Models trained solely with rheological measurements without including formal parameters were able to achieve high prediction accuracy. The printability of the developed Aloe gel polysaccharide ink was found to be predictable at 82% for width and roughness labels and 88% for overall printability labels. This study allows the model to be generalized to 3D food printing inks of various compositions and is promising when exploring the use of these materials in 3D food printing binder spray additive manufacturing technologies such as alternative foods and nanofoods.*

KEYWORDS *3D Food Printing,Alternative Foods, Nanofoods, Aloe Gel-based Food Inks, Aloe Gel Polysaccharide, Aloe Gel Pectin (AGP), Aloe Gel Cellulose Nanoparticle (AGCN),AILearning; Printability, Rheological Measurements.*

I. INTRODUCTION

3D food printing is an emerging concept for precision modular food manufacturing to address the need to customize food according to individual preferences and nutritional requirements [1]. Among the various 3D food printing technologies studied for food applications, extrusion-based 3D food printing is the most widely used technology [2, 3, 18]. This technique has the versatility to 3D print different types of food materials, such as bottom-up process of nanofoods and nutrient delivery systems [19, 20], hot-melt extrusion of chocolate [4], room-temperature extrusion of dough, frosting, and Nutella etc. [5, 6], as well as extrusion of food hydrocolloids [7, 8]. Food-grade hydrocolloid agents, such as various polysaccharides, can either be crosslinked to form gels via chemical modification [9] or ionic complexation [10], or added as thickening agents to modify food

properties [11].Previous studies have demonstrated the potential of developing 3D food printed structures using hydrogels composed of starch [13], agar [8], alginate [12], pectin [13] or other polysaccharide-based 3D food printing inks [14, 21]. However, achieving optimal compositions for a reproducible and high-resolution printing remains a significant challenge. The challenges result from the lack of comprehensive understanding of a relationship between formulation parameters, rheological properties, and printability features.As a result, previous studies have used empirical approaches to explore 3D food printing ink formulations and their application to print diverse structures [16, 18-21, 22]. The trial-and-error procedure for formulation optimization of food inks is time consuming and often only applicable to a specific ink composition, limiting the applications of 3D printing in food systems.

Hydrogels qualified as good3D food printing inks should have two basic characteristics: extrudability and post-printing stackability [23]. Rheology is a common characterization for hydrogel-based 3D printing inks and has been reported in most of the ink development studies. A few studies have evaluated the relationship between formulation parameters and rheological measurements of 3D food printing inks [10, 17, 24]. The results of these studies illustrate that the rheological properties of hydrogels largely depend on the chemical nature and concentration of the polymers, gelling mechanisms, and the extent of crosslinking within the polymer networks. However, most of the studies used subjective evaluation to assess the printability of 3D food printing inks through experimental observations [5, 6, 24, 25, 26].The lack of quantitative criteria for printability assessment prevents the development of predictive relationships between 3D food printing inks' properties and printability. Conventionally, printability of inks is assessed by shape fidelity, i.e. the extent of spreading and fusion of the printed filaments, measured either manually [26]or through image analysis [23, 27, 28]. However, not many studies have focused on assessing the smoothness of 3D food printing ink deposition except visual inspection during printing.

This study developed two printability assessment metrics: printed filaments' width and roughness and used these metrices to evaluate the printability of polysaccharide-based 3D food printing inks using machine learning and response surface methodology (RSM) with regression. Aloe gel pectin (AGP) and Aloe gel cellulose nanoparticle (AGCN) were selected to formulate the polysaccharide-based 3D food printing inks with ionic crosslinking. Pectin and cellulose are the major constituents of plant cell wall [29] and the developed 3D food printing inks could be used to print plant-based food simulants. Pectin is a family of heterogeneous polysaccharides rich in galacturonic acid, a proportion of which could be methyl esterified. AGP has a low degree of methoxylation and AGP gels are generally formed through electrostatic complexation with cations such as Ca^{2+}. The polymeric network generated by crosslinking of AGP with calcium ions is responsible for maintaining the 3D structure of the 3D food printing ink hydrogels formulated in the current study. AGCN was incorporated into the gels as a minor component to modify the mechanical properties of the 3D food printing inks [19-21, 30, 31]. 3D food printing inks with different concentrations of AGP, AGCN and $CaCl_2$ were formulated and characterized for their rheological properties.The formulated inks were printed using an extrusion-based 3D printer and quantitative metrics were established to assess the inks' printability. Response surface methodology (RSM) was used to investigate the relationship between the ink compositions and rheological properties and printability metrics. A few studies in tissue engineering utilized RSM [25, 32]or AI machine learning techniques [33] to model the relationship between 3D printing parameters and printability, but were limited to a single ink composition variable and did not incorporate rheological measurements in the models. Complementary to RSM and regression analysis, AI machine learning approach using random forest models were trained to predict the printability from inks' compositions and rheological measurements.

In our previous research, we designed the 3D printing process for NDS(Nutritional Delivery System) and nanofoods as shown in **Fig. 1** and manufactured alternative foods through sequential layering and spraying processes[15, 18-21].Therefore, in this study we built a predictive model that 3D food printing links the composition and rheological properties of the ink to carefully defined printability metrics. This allows 3D food printing ink formulation optimization to be performed more efficiently compared to heuristic approaches. The development of these predictive relationships could help evaluate both the quality of 3D food printing structures and the transformation of these 3D food printing inks to produce alternative and functional foods, such as NDS and nanofoods, with tailored sensory and nutritional profiles.

II. RESEARCH METHODS

A. Materials and 3D Printing Food Ink Preparation

Super Green Vera Aloe Gel Powder[TM], provided by KimJungMoon Aloe (Jeju, Korea), was used as the source of Aloe gel pectin (AGP). As specified by the supplier, the product contains 86.3 wt% of AGP-KJM (degree of esterification 7%) and 13.7 wt% added dextrose. Aloe gel cellulose nanoparticle (AGCN) was purchased from KJMbio Lab (Seoul, Korea), with width: 5–20 nm and length: 100–250 nm. Calcium chloride and sodium tetraborate decahydrate were purchased from Sigma-Aldrich (St. Louis, USA). Sulfamic acid was purchased from EMD Millipore Corporation (Billerica, USA). Sulfuric acid and sodium hydroxide were

purchased from Fisher Scientific (Pittsburg, USA). 3-phenylphenol (m-hydroxydiphenyl) was purchased from Spectrum Chemical Mfg. Corp. (New Brunswick, USA). Ultrapure water (18 MΩ cm) was obtained using the in lab Milli-Q RG water ultra-purification system from EMD Millipore (Billerica, USA).

The 3D food printing inks were formulated as hydrogels composed of different concentrations of AGP, AGCN, and $CaCl_2$. Total polysaccharide (Uni-pectine^{TM}(g) / Uni-pectine^{TM}(g) in regression models), and calcium crosslinking density (R) were the three formulation parameters used in the experimental design, as summarized in **Table 1**.The crosslink density was defined as the stoichiometric ratio between the molarity of Ca^{2+} and that of COO^- (R = 2[Ca^{2+}]/[COO^-]). The molarity of $COO^-$was calculated as [COO^-]= [*uronic acid*]*(1 -*degreeofmethoxylation*). The Uni-pectin^{TM}contained 1.92 mmol galacturonic acid equivalence per gram, measured using a colorimetric assay, as described in previous studies [34, 35]. For each 3D food printing ink formula, $CaCl_2$ solution with different concentrations were prepared based on the specified Uni-pectine^{TM} concentration, crosslinking density (R), and the measured total uronic acid content.

Table 1. 3D food printing ink formulation parameters used in the Box-Behnken design

Formulation parameters	Low	Medium	High
Total polysaccharide	3 %	4.5 %	6 %
Uni-pectin : AGCN	6 : 4	8 : 2	10 : 0
R = 2*[Ca^{2+}]/[COO^-]	0.35	0.45	0.55

The Uni-pectine^{TM} solution (referred to as pectin solution hereafter) with concentrations levels of 4.29, 6.43, 8.57 wt% were prepared by dissolving the pectin powder in 80 °C water and heated for 10 min, then continuous stirring for 2 h while cooling to ensure fully hydration. AGCN was adjusted to 3, 4.5, and 6 wt% respectively. The prepared pectin solution and $CaCl_2$ solution were separately loaded into two syringes, connected with a Luer-lock connector, and mixed at a volumetric ratio of 7 to 3 to form gels with different strength as determined by the pectin concentration and crosslinking density. The resulting pectin gel was then mixed thoroughly with AGCN of the corresponding concentration at different ratios as specified in the experiment design. Bubble generation was avoided at best during mixing. The final food inks were stored at 4 ° C and used for 3D printing and rheological measurements between 12 and 48 h after preparation.

B. Rheological Measurements
The developed 3D printing food inks are non-Newtonian hydrogels whose rheological properties largely affected their behavior before, during and after 3D printing. To investigate the effect of the three formulation parameters on the food inks, three rheological tests were performed: *(1) steadystate flow test; (2) dynamic viscoelastic properties test; and (3) recovery test.* The rheological measurements were conducted using an MCR 302 stress-controlled rheometer (Anton-Paar, Austria) equipped with a 25 mm parallel plate and a 0.55 mm measurement gap, at 25 ± 0.1 °C.

B-1. Steady-State Flow Test
The shear thinning property of food inks was evaluated using a steady-state flow test. Shear stress was recorded while changing the shear rate in the range of 0.1 s^{-1} to 100 s^{-1}. The results were then fitted using the Herschel-Bulkley equation:

$$\tau = \tau_0 + k\dot{\gamma}^n$$

where τ is the shear stress, $\dot{\gamma}$ the shear rate, k the consistency index, and n the flow index. Fluids with $n < 1$ are shear-thinning, with n greater than 1 are shear-thickening, and $n = 1$ indicating Newtonian flow behavior.

B-2. Dynamic Viscoelastic Properties Test
Storage modulus (G') and loss modulus (G") as a function of increasing strain (γ_0) and angular frequency (ω) was measured for all 3D food printing inks. Amplitude sweeps were performed in the range of 0.01 to 100% strain atω = 1 rads/s (0.16 Hz) to determine the linear viscoelastic region. The upper limit of the linear viscoelastic region, referred to as the linearity limit, was the strain above which the hydrogel collapsed

and the storage modulus dropped to 95% of the plateau value at low strain amplitudes. The shear stress at the linearity limit was the yield stress (τy). The shear stress at the crossover between G' and G" curves was defined as the flow stress (τf). The region between τy and τf could be considered as the transition region of the hydrogel from an elastic solid to a viscous liquid. A flow transition index ($\tau f / \tau y$) was defined to indicate the width of this range. Frequency sweeps were performed from 0.06 to 100 rad/s at 1% strain (within the linear viscoelastic region for all 3D food printing inks) to determine the frequency dependency of G' and G", and the phase angle δ. Loss factor $\tan(\delta) = G''/G'$ was calculated at 0.1 rad/s, as an indicator of the gelation state of a hydrogel, where lower valuesand more elastic gels suggested highly crosslinked [32].

B-3. Recovery Test

The thixotropic properties and recoverability of the 3D food printing inks were evaluated in a threestep recovery test. The viscosity of hydrogels was measured as the shear rate underwent a threestep change: 0.1 s^{-1} for 60 s (step 1), 600 s^{-1} for 10 s (step 2), and again 0.1 s^{-1} for 60 s (step 3). The three steps simulated a low-high-low shear rate change similar to the shear rate experience by the 3D food printing ink before, during, and after the extrusion step during 3D printing. A recovery index was calculated as the ratio between the mean viscosity during step 3 to that during step 1.

C. 3D Food Printing and Printability Assessment

In this study, the 3D food printing inks were printed using a Print2taste Mycusini inkjet printer (Mycusini Inc., Germany). 25-gauge nozzles (i.d. 0.26 mm) were used for printing. Extrusion pressure, layer height, nozzle moving velocity, and the printing pattern were manipulated using the Allevi online software. The printer settings were tuned for each 3D foodprinting ink. The optimal pressure was the minimum pressure needed to extrude a continuous filament with relatively uniform diameter. The layer height and nozzle moving velocity were adjusted so that the printed filament could be continuously deposited on a glass slide.

To assess the printability of the 3D food printing inks, the printed filaments were imaged using an optical microscope (Olympus IX71) with a 4x magnification objective lens. Two measurements were used as the criteria for printability assessment: *filament width and roughness.***Fig. 1** showed a schematic diagram of how these two measurements were extracted from the bright field images of printed filaments. The images were first rotated so that all the filaments in the images aligned along the X direction (horizontally), then thresholder and binarized to detect the edges of the filaments. The centerline of a filament was generated by connecting the midpoints of the vertical segments between the upper and lower edges. Then linear trendlines were fitted to the upper edge, the center line, and the lower edge, respectively. At 10 equally spaced points along the center trendline, perpendicular segments were drawn until they intersected with the upper and lower edges. Filament width was calculated as the average length of these 10 segments. A relative width was calculated as:
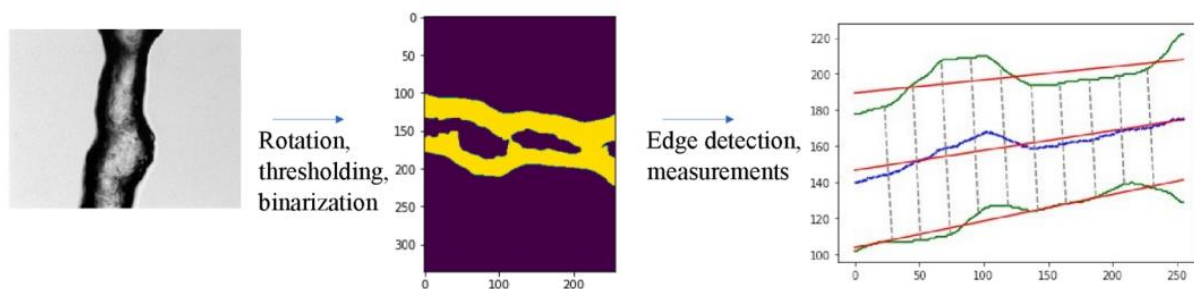

Fig.1. Schematic diagram of measuring the printed filament width and roughness through image analysis

$$Relative width = measured width - target width / target width \quad (2)$$

The where the target width was the inner diameter of the nozzle: 260µ m. Roughness of printed filaments was calculated according to *Equation (3)*. Filament roughness was defined as the mean squared error between the y coordinates of detected edges and those of their corresponding fitted trendlines, then averaged for upper and lower edges:

$$Roughness = 1/2 \sum\nolimits^{(2/l=1)} - 1/n \sum\nolimits^{(n/i=1)} (yi^{edgel} - yi^{trendline1})^2 \quad (3)$$

$(xi^{edgel} - yi^{edgel})^2$ are coordinates of points on the upper edge of the filament when l = 1 and the lower edge when l = 2.$(xi^{trendline1} - yi^{trendline1})^2$ are coordinates on trend lines defined in the same way. n is the total number of pixels along the × direction. 5 images were taken at different locations on one printed filament, and both filament width and roughness measurements were averaged over the 5 images. The image analysis was

conducted in Python. Based on the relative width and roughness measurements, binary labels were generated for each of these two metrics with pre-specified thresholds. Moreover, as a final printability assessment combining both metrics, a binary ink quality label was generated:a good ink should be printed with high resolution (close to the target width) and smoothness (low roughness). The criteria for classification of the ink formulations and their corresponding labels for the three printability assessment metrics are presented in **Table S1**.5 mm[*]5 mm[*]5 mm grid cubes and 8 mm[*]8 mm 3-layer grids, both with 1 mm line spacing were printed using different food inks for visual inspection. The optimized printing setting for each ink was used. The printed structures were inspected for defects such as line fusion, interrupted extrusion, shape deformation, etc. After printing, the printed objects were submerged in 90 mM $CaCl_2$ solution for 10 min for post-printing crosslinking.

D. Experimental Design and Model Construction

A Box-Behnken experimental design was adopted using the 3 formulation parameters given in **Table 1**. This resulted in 15 inks with 13 different compositions (**Table S2**). Triplicates of the food inks were prepared independently for the rheological measurements, printability assessment, and 3D printing inspection.

Pairwise Pearson's correlation and principal component analysis (PCA) was conducted on all the rheological measurements: the flow index (n) from the fitted Herschel-Bulkley equation, storage and loss modulus (G', G"), loss factor ($\tan(\delta)$), yield stress (τY), flow transition index, and recovery index. Four response variables (Y): the first two principal components of the rheology PCA model, together with the printability assessment measurements: filament width and roughness, were separately regressed on to the three formulation parameters (total polysaccharides: X1, pectin fraction: X2, crosslinking density: X3) and their two-way interaction terms:

$$Y = \beta_0 + \beta_1 X1 + \beta_2 X2 + \beta_3 X3 + [\beta_4 X1X2 + \beta_5 X1X3 + \beta_6 X2X3] + \epsilon (4)$$

Given the normality assumption behind the *p*-value calculation of the regression coefficients, filament width and roughness were log transformed before fitting the regression models. Ordinary least square regression (OLS) with Akaike information criterion (AIC)-based stepwise model selection was used to determine which interaction terms to include in the regression model.

To better predict the ink printability and explore the possibility of generalizing the model beyond current formulation parameters, random forest classification models were built to predict the width label and roughness label. Different feature sets composed of the 3D food printing inks' rheological properties and/or the formulation parameters were constructed to train the classification model. Given the small sample size, stratified repeated 5-fold cross validation was used to train and test the models. Stratification based on the response labels guaranteed that the ratio between label classes was the same in the train and test set for every train-test split during cross validation. The cross-validation classification accuracy for each feature set and response variable were reported. To predict the binary 3D food printing ink quality label, both a direct and an indirect approach were taken. For a direct prediction, the binary quality label was predicted as the response variable in the same way using cross validation. The indirect approach combined the prediction results from the previously trained models on width label and roughness label to obtain a predicted binary quality label in the same way as the true binary quality label was generated. The regression analysis was conducted in R (version 4.1.3) and the random forest models were constructed using the scikit-learn library in Python (version 3.7.10).

III. RESULTS

A. Rheological Properties of LMP-CNC-CaCl₃D Food PrintingInks

Based on a Box-Behnken design, 13 different food ink formulations (**Table S2**) with three components: AGP, AGCN, and $CaCl_2$ were developed. The ranges of total polysaccharides concentration and cross-linking density were chosen based on alginate or pectin-based bioink formulations reported in previous studies and preliminary experiments [32, 36]. These formulations were evaluated for rheological characteristics, including the shear-thinning, viscoelastic, and thixotropic properties of the hydrogel-based inks.

A-1. Shear-Thinning Properties of 3D Food Printing Inks

In the steady-state flow test, the viscosity of all the 3D food printing inks decreased with the increasing shear rate in the range from 0.1 s^{-1} to 100 s^{-1}, indicating a shear thinning behavior. **Fig. 2** demonstrates such a shear thinning behavior of three representative formulations. After fitting the shear stress (τ) vs. shear rate (γ') data to the Herschel-Bulkley equation (*Equation (1)* the flow index (n) of all samples were smaller than one (**Table S3**), confirming their pseudoplastic nature.
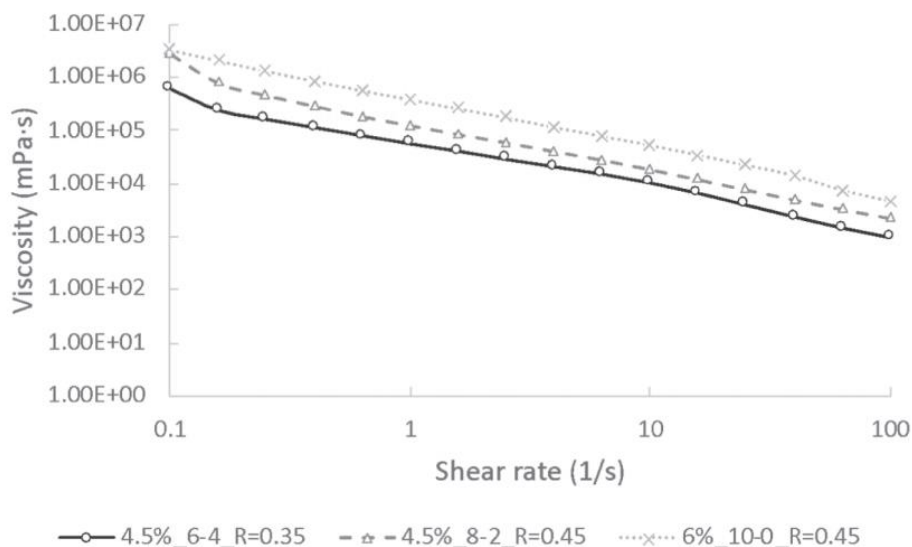
Fig. 2. Shear thinning property of three representative bioinks: 3% total polysaccharides/6-4 pectin-to-AGCN ratio/R = 0.45 crosslinking density (4.5%/6-4/R = 0.35); 4.5%/8-2/R = 0.45; 6%/10-0/R = 0.45

A-2. Viscoelastic Properties of 3D Food PrintingInks

The evolution of storage (G') and loss (G'') moduli of 3D food printing inks during the strain amplitude sweep are shown in **Fig. 3**. Storage and loss modulus indicate the elastic and viscous components of a material respectively. The linear viscoelastic region of the 3D food printing ink compositions was found below 10% strain amplitude, above which the gels collapsed and large reduction in G' was observed. Above the linearity limit, G' decreased monotonically, while G'' increased first before it started to decrease. This phenomenon is described as the weak strain overshoot under large amplitude oscillatory shear (LAOS) (Hyunetal.,2002). Such a phenomenon was observed for all food inks except 3%_8-2_R = 0.35, which contained 3% total polysaccharides, 8-2 AGP-to-AGCNNC ratio, and crosslinking density of 0.35. **Table S3** summarizes the yield stress and flow transition index of the 3D food printing inks developed in this study. Yield stress can be correlated with the amount of pressure needed to initiate the flow of gels during extrusion. The flow transition index reflects the brittleness of the hydrogels: the closer is the index to 1, the higher is the tendency of the hydrogel to brittle fracturing [37]. Higher total polysaccharides content, higher pectin fraction, and higher crosslinking density all led to a larger yield stress and a narrower flow transition region.
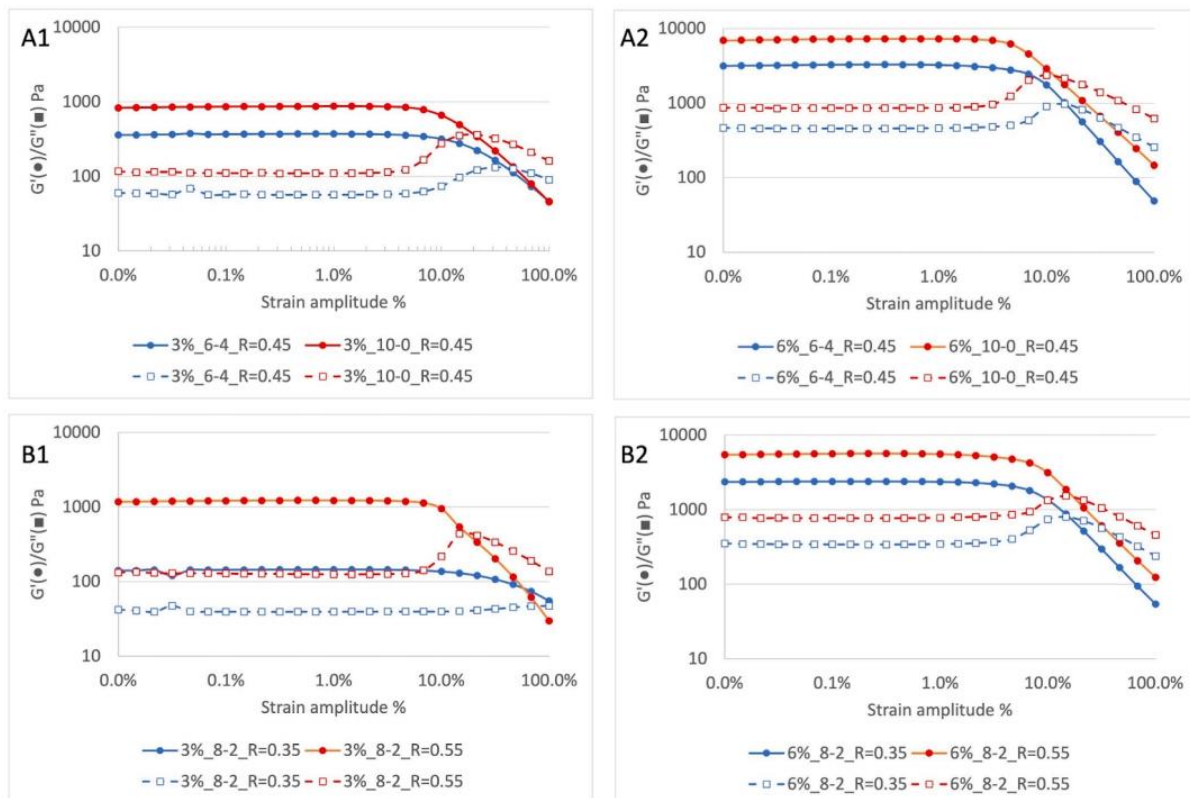
Fig. 3. Storage modulus G' (solid line) and loss modulus G" (dashed line) vs. strain amplitude at $\omega = 1$ rad/s for 3D food printing inks composed of 3% (A1, B1) and 6% (A2, B2) total polysaccharides. Subplots A1 and A2 showed the effect of different pectin-to-AGCN ratio; subplots B1 and B2 showed the effect of different crosslinking density

Fig. 4 shows the dependency of G' and G" on the oscillation frequency for the same set of 3D food printing inks, in the range of 0.06 ~ 100 rad/s. In this range, G' dominated G" and was relatively frequency-independent for almost all the 3D food printing inks, indicating that the gels behaved like an elastic solid, which is common for a covalently cross-linked interwoven polymer network [38].As shown in **Table S3**, all the 3D food printing inks with crosslinking density R = 0.55 had loss factor smaller than 0.1, and all the ones with R = 0.35 had loss factor greater than 0.1 or 0.2. Loss factor reflects the gelation state of hydrogels and small loss factor suggests the predominance of the elastic behavior in the material, due to a stronger and a more crosslinked gel [39].

A-3. Thixotropy of Food PrintingInks

Thixotropy of 3D food printing inks was tested in a three-step recovery test. When experience a high shear rate, all 3D food printing inks showed a rapid decrease in viscosity as expected given their shear thinning nature. The ability of the material to recover and regain its initial viscosity after removal of the large shear rate suggested how likely the printed filaments would spread after printing, thus was regarded as an indicator of shape fidelity of the printed objects. **Fig. 5** shows the viscosity change of the three representative 3D food printing inks during the three-step recovery test: 4.55/6-4/R = 0.35, 4.5%/8-2/0.45, and 6%/10-0/0.45. It could be observed that 3D food printing ink 4.5%/6-4/0.35 required a longer time to recover to an equilibrium viscosity after entering step 3, compared with the other two 3D food printing inks. Also, as shown in **Table S3**, among the three 3D food printing inks, 6%/10-0/0.45 had the highest recovery index, defined as the ratio between the mean viscosity during step 3 to that during step 1, followed by 4.5%/8-2/0.45, while 4.5%/6-4/0.35 was the lowest. Inks with low recovery index and longer recovery time were more susceptible to spreading post printing, resulting in poor shape fidelity.
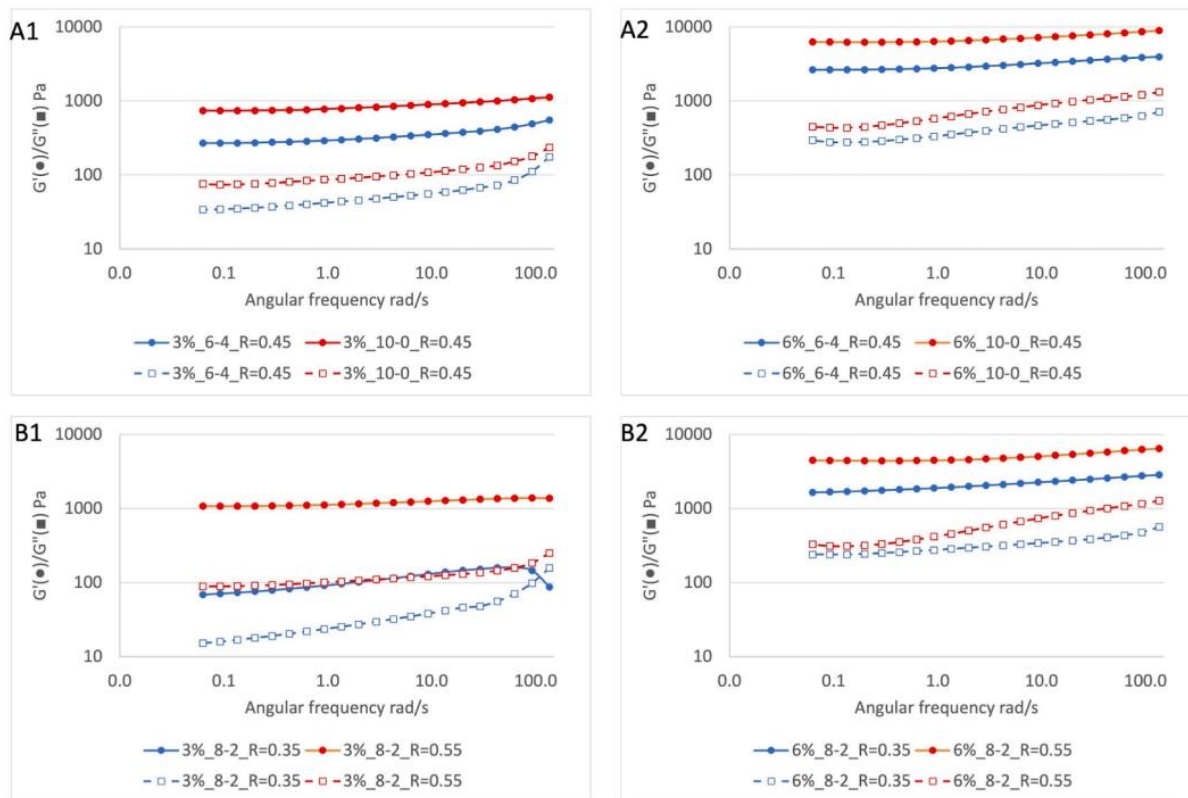
Fig. 4. Storage modulus G' (solid line) and loss modulus G" (dashed line) vs. angular frequency at 1% strain amplitude for 3D food printing inks composed of 3% (A1, B1) and 6% (A2, B2) total polysaccharides. Subplots A1 and A2 showed the effect of different pectin-to-AGCN ratio; subplots B1 and B2 showed the effect of different crosslinking density
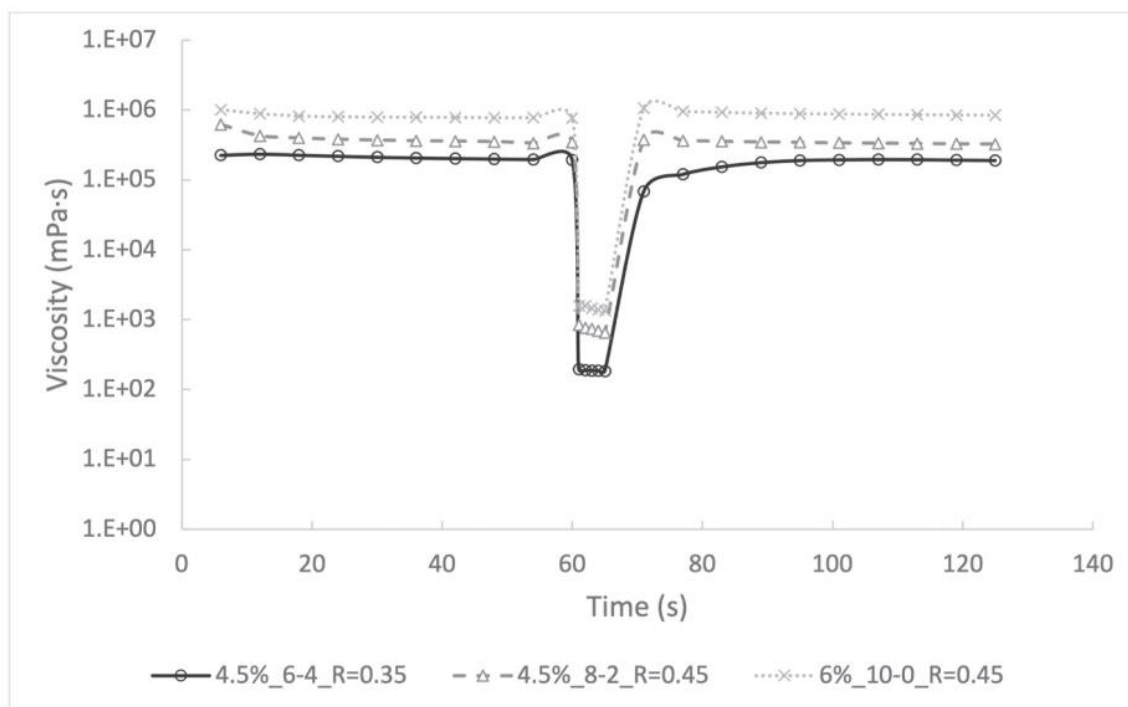

Fig. 5. Viscosity recovery of bioinks: 3% total polysaccharides/6–4 pectin-to-AGCN ratio/R = 0.45 crosslinking density (4.5%/6–4/R = 0.35); 4.5%/8–2/R = 0.45; 6%/10–0/R = 0.45. The three-step recovery test measured viscosity of bioinks at 0.1, 600, and 0.1 s− 1 shear rate respectively to mimic the before, during, and after printing status

B. 3D Printing and Printability Characterization

      The 13 3D food printing ink formulations were printed into filaments using the printing parameters optimized for each ink, as specified in **Table S4**. All the 3D food printing inks were printed with the same nozzle moving speed (6 mm/s) but with different extrusion pressure and layer height (the distance in z direction that the nozzle moved up after printing each layer). The extrusion pressure was tuned to address variations in the rheological characteristics of the 3D food printing inks and the layer height was adjusted to account for the different degrees of expansion of the printed filaments upon extrusion. The printing parameters used for these inks generally were in range of 15 ~ 25 psi of pressure and 0.31 ~ 0.35 mm layer height (**Table S4**). During printing, it was observed that most of the inks were deposited with some lag time after the pressure was applied, due to their viscoelastic nature. Three ink formulations appeared to be very thin and experienced extensive spreading after deposition: 3%/6-4/R = 0.45, 3%/8-2/0.35, and .5%/6-4/0.35. The 3D food printing ink formulations with the following compositions 4.5%/10-0/0.55, 6%/10-0/0.45, 6%/8-2/0.55 formed strong gels that required very high pressure to overcome the initial yield stress to flow (**Table S4**). The deposition of these 3D food printing inks was unsmooth and inconsistent, often resulting in broken filaments. Two of the 3D food printing inks with 3% total polysaccharides: 3%/10–0/0.45, 3%/8–2/0.55, although did not require high extrusion pressure, exhibited un-smoothness during printing. The rest of the 3D food printing inks could be successfully printed with a continuous deposition and good shape fidelity based on visual observation. Besides the visual inspection, the printed filaments were imaged under optical microscope and measured for filament width and roughness, as summarized in **Table S3**. **Fig. 6** shows a scatterplot of filament roughness vs. relative width together with the thresholds selected to binarize these two metrics. The threshold levels were determined based on preliminary experiments (**Table S1**). Samples falling into each of the four width-roughness label combinations were color-coded and kernel density estimation plots were used to visualize the distribution of inks in each group based on the selected 3D food printing ink printability metrics.
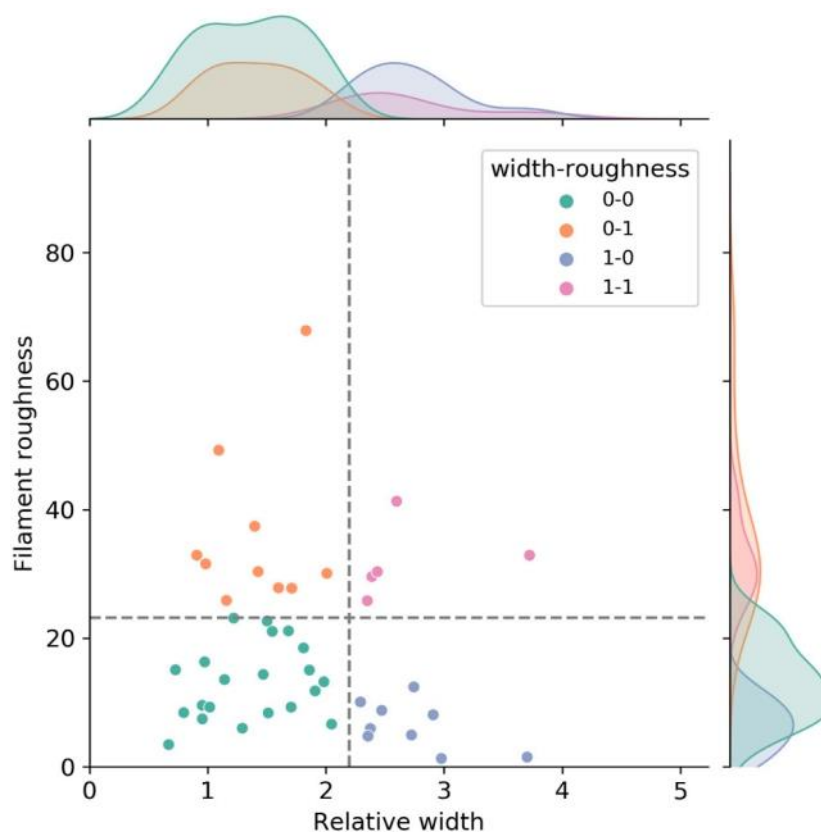

Fig. 6. Scatterplot of filament roughness vs. relative width, color-coded by the width-roughness combination label. The dashed lines indicated the thresholds used to binarize the two metrics. The kernel density estimation plots were used to visualize the distribution of 3D food printing inks in each group regarding the two metrics

To demonstrate the ability of the developed 3D food printing inks for high-resolution printing, three 3D food printing ink formulations with width-roughness label of 1-0, 0-0, and 0-1 respectively were selected for test printing of a 3D structure: 4.5% /6-4/R = 0.35, 4.5%/8-2/0.45, and 6%/10-0/0.45. With each 3D food printing ink, a 5^*5^*5 mm^3 3D grid structure with 1 mm line space (**Fig. 7 A-C**) and an 8 mm* 8 mm 3-layer grid with 1 mm spacing (**Fig. 7 D-F**) was printed. Both the 3D grid cubes and the 3-layer grid structures were submerged in 90 mM CaCl$_2$ solution after printing. The dimensions of the objects shown in Fig. 7 were smaller than the designed values due to shrinkage after crosslinking. Although the deposition of 3D food printing ink 4.5%/6-4/0.35 was smooth and uniform, the 3D grid cube printed with this 3D food printing ink showed round edges and as more layers were deposited, the base of the cube partially collapsed under the influence of gravity, indicating low shape fidelity. **Fig. 7 D-F** are top views of the 3-layer grids printed with the three 3D food printing ink formulations, illustrating whether the filaments within a grid fused together when printed at a 1 mm line spacing. Based on the observations, we concluded that formulation 4.5%/6-4/0.35 was too thin to be suitable 3D food printing inks. On the contrary, formulation 6%/10-0/0.45 could not be deposited smoothly and intermittent breaking of filaments were observed during printing. As a result, the printed objects (**Fig. 7 C, F**) showed apparent defects. Formulation 4.5%/8-2/0.45 could be deposited regularly and uniformly, and the printed structures showed clean and sharp edges, the 1 mm line spacing was well-maintained as designed as well. Smooth deposition and high shape fidelity make this formulation a good candidate for 3D printing.
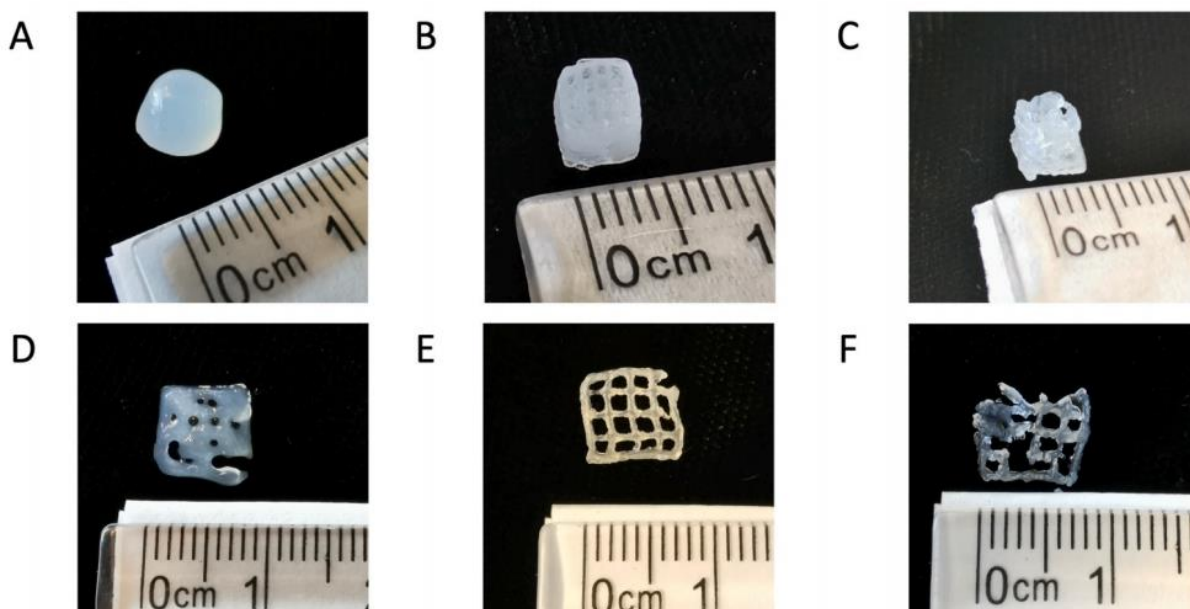

Fig. 7. Representative samples of printed grid cubes (5^*5^*5 mm3 with 1 mm gap) (A, B, C) and 3-layer grids (8^*8 mm^2 with 1 mm gap) (D, E, F) using three food ink formulas: (A, D). 4.5% total polysaccharides/6-4 pectin-to-AGCN ratio/R = 0.35 crosslinking density (width-roughness label 1–0); (B, E) 4.5%/8–2/R = 0.45 (width-roughness label 0–0); (C, F) 6%/10–0/R = 0.45 (width-roughness label 0–1)

C. Regression models of rheological properties and printability measurements on 3D food printing ink formulation parameters

As shown in **Fig. 8A**, many of the rheological characteristics were significantly correlated. For example, the strong positive correlation among storage modulus, loss modulus, yield stress, and recovery index confirmed that these measurements were all positively associated with stronger gels. Additionally, stronger gels would have lower loss factor and shorter flow transition region, which are negatively correlated with the other rheological measurements. Flow index did not have significant correlation with any of the other rheological characterizations. Due to the high collinearity, PCA was implemented to reduce dimension of the variable space and determine the principal components of rheological measurements. The PCA biplot (**Fig. 8B**) showed that most of the rheological measurements had high loadings in the space of the first principal component (PC), except the fitted flow index (*n*), which was more associated with the second PC. This was consistent with the insignificant correlation between flow index and other variables. The first two PCs accounted for 57.9% and 16.6% of the total variance and the first four PCs accounted for more than 90% of the total variance (**Fig. 8C**).

RSM was used to investigate the effect of the formulation parameters on the rheological and printability measurements. The response surfaces for log(filament width), log(filament roughness), and the first 2 PCs from the PCA of rheological measurements were constructed based on the least square regression models as specified in *Equation (4)*.The regression coefficients (β1 β6 in Equation (4), their p-values and R2 of the models are summarized in **Table 2. Fig. 9** displays the response surface plots of the four response variables as a function of the total polysaccharides and the crosslinking density at different pectin fraction levels. It could be observed from the response surface plots for log (filament width) (**Fig. 9A**) that it decreased with increasing total polysaccharides, pectin fraction, and crosslinking density.The response surfaces had some curvature: a steeper reduction in filament width was observed with increasing total polysaccharides at lower crosslinking density; the effect of increasing crosslinking density on reducing filament width was more obvious at lower total polysaccharides concentration and lower pectin fraction. The observations were consistent with the regression coefficients from the least square regression model in **Table 2**.The main effects of the three formulation parameters on filament width were all significant. Two interaction terms: total polysaccharides - crosslinking density, pectin fraction - crosslinking density included in the final model, although not significant, did improve the overall model quality.
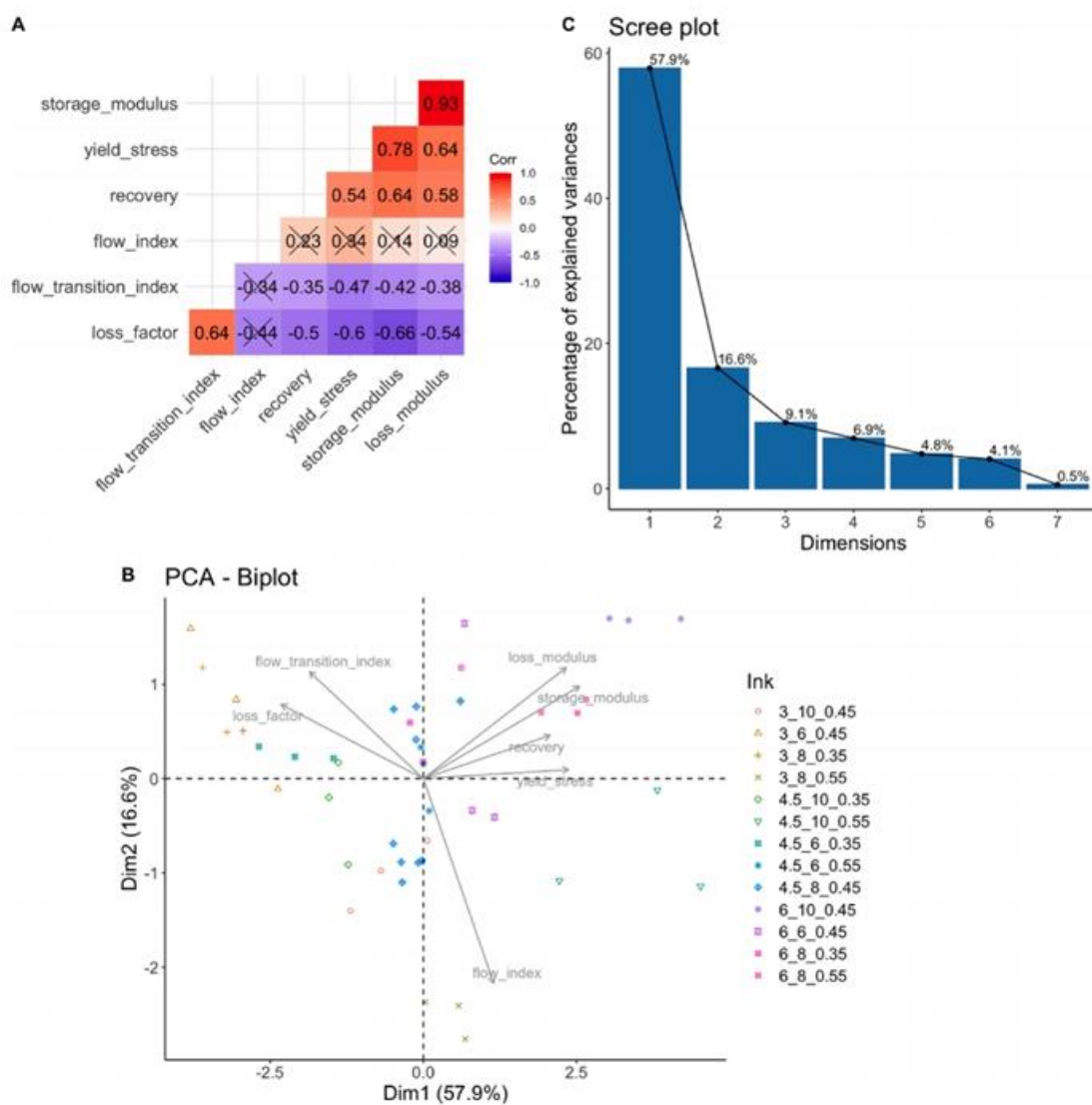

Fig.8. Correlation matrix (A), PCA biplot (B), and PCA scree plot (C) of the rheological characterizations of 3D food printing inks. The correlation indices were crossed out if the correlation was not significant (p greater than 0.05) for the pair of variables
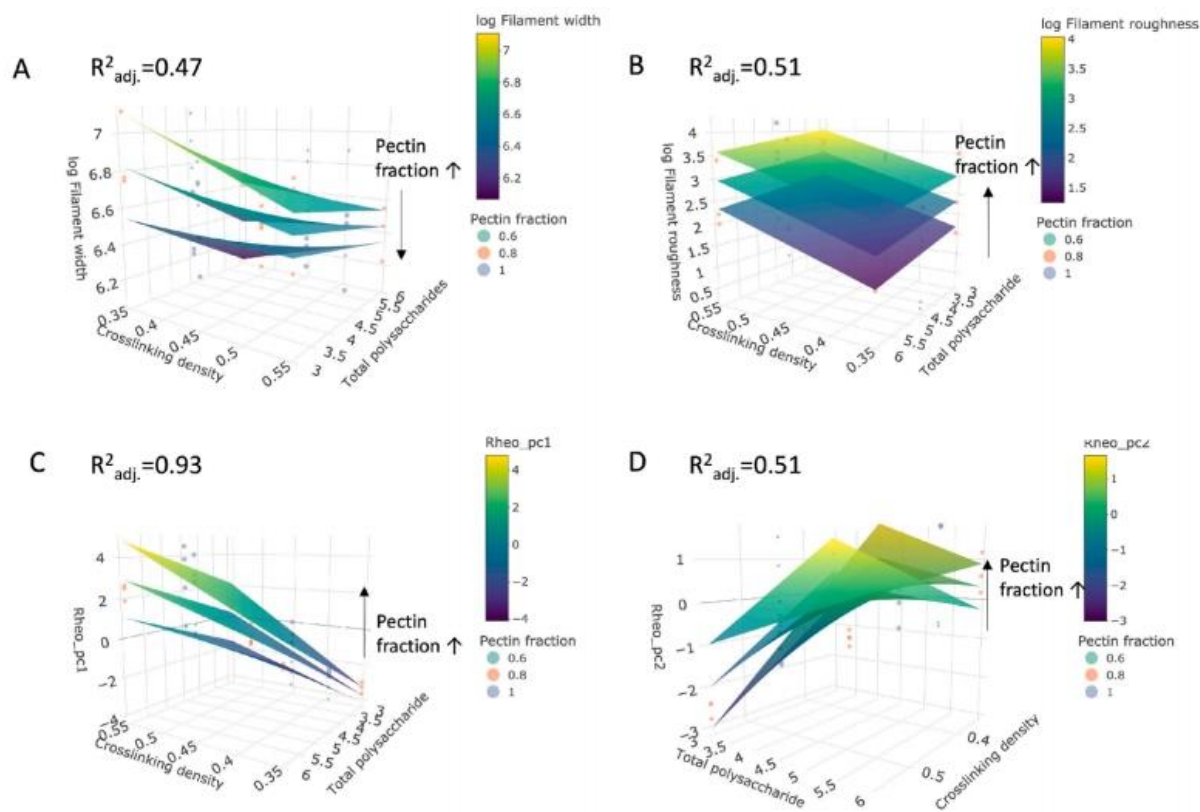
Fig. 9. Response surface plots of (A) printed filament width, (B) filament roughness, (C) rheo_PC1, and (D) rheo_PC2 as a function of formula parameters. The orientation of the axis of the 3D plots was adjusted to better visualize the response surfaces

The response surface plot for log(filament roughness) (**Fig. 9B**) shows that it was positively associated with increasing pectin fraction and crosslinking density but not significantly influenced by the total polysaccharides, and the surfaces were flat and parallel, indicating little interaction effects. The 1st principal component of rheological measurements, PCA (rheo_PC1) was positively associated with total polysaccharides, pectin fraction, and crosslinking density (**Fig. 9C**). **Table 2** shows that the regression coefficient for total polysaccharides is positive and significant, consistent with the response surface plots. However, the regression coefficients of crosslinking density and pectin fraction on rheo_PC1 were both negative, opposite to what was observed in **Fig. 9C**. This could be attributed to the significant interaction term between crosslinking density and pectin fraction, which has a large effect size. As a result, after accounting for the interaction terms ($X2^*X3$ in *Equation (4)*, the effect size of each individual variable (X2, X3) would diminish or even have a reversed sign. Rheo_PC2 response surfaces (**Fig. 9D**) show strong interactions among formulation parameters and one relatively clear trend was that at the lowest total polysaccharides level, rheo_PC2 decreased with increasing crosslinking density and increasing pectin fraction. Among the four response variables, rheo_PC1 was the most well-explained by the linear regression model, with the highest adjusted R^2 score of 0.93. All the other response variables were not very well-explained since their adjusted R^2 was only around 0.5. The unexplained variance could be attributed to nonlinear relationships between the formulation parameters and the response variables and high-order terms that were not included in the current model *Equation (4)*.

D. Machine learning enabled prediction of 3D food printing inks' printability

As shown in **Fig. 8A**, many of the rheological characteristics were significantly correlated. For example, the strong positive correlation among storage modulus, loss modulus, yield stress, and recovery index confirmed that these measurements were all positively associated with stronger gels. Additionally, stronger gels would haveThe RSM results reflected that the formulation parameters had a linear relationship with Rheo_PC1 (adj. R2 = 0.93), but not with the printability metrics, indicating the need for nonlinear models. Therefore, we constructed random forest classification models to predict the ink's width and roughness labels, as well as the binary quality label, classified using criteria described in **Table S1**. Three feature sets were used to predict the

labels: rheological measurements + formulation parameters, formulation parameters alone, or rheological measurements alone. **Table 3** summarizes the cross-validation prediction accuracy for the random forest classifiers on each label using the three feature sets. The prediction accuracy did not show a sizable difference between classifiers trained with the rheological measurements alone or with formulation + rheology. However, training with formulation parameters alone resulted in 5 ~ 10% lower accuracy compared to the other two feature sets.

Table 2. Regression coefficients, p-values and adjusted R^2 of the ordinary least-square regression models of filament width, roughness, rheo_pc1, and rheo_pc2 as response variables, and formula parameters as covariates

Term	Filament width [a]			Filament roughness [a]			Rheo_PC1			Rheo_PC2	
	Estimate	P-value		Estimate	P-value		Estimate	P-value		Estimate	P-value
Intercept	10.7	3.13e-10*		−1.62	0.0574		−5.14	0.0689		15.3	8.48e-3*
Total polysaccharide	−0.347	0.0463*		−0.151	0.0719		1.29	<2e-16*		−4.20	1.87e-5*
Pectin fraction	−3.01	0.0221*		3.11	8.49e-6*		−9.14	9.63e-3*		−2.78	0.634
Crosslinking density R	−6.43	0.0273*		5.45	6.32e-5*		−9.30	0.129		−17.7	0.108
TotalPS:PC_frac[b]	/	/		/	/		/	/		2.26	2.83e-3*
TotalPS:R[b]	0.5378	0.154		/	/		/	/		5.96	1.50e-4*
PC_frac:R[b]	4.60	0.105		/	/		30.0	2.16e-4*		−17.9	0.0999
Adjusted R^2	0.47			0.51			0.93			0.51	

[a] log transformation was performed on filament width and roughness before regression.
[b] Coefficients of interaction terms excluded from the final model after the AIC guided model selection process were not shown.

Table 3. Cross validation classification accuracy (mean ± sd) for the width and roughness label, and the binary quality label using different feature sets

Ink quality metrics	Feature set	Data split	Accuracy
Relative filament width	Formula + rheology	Train	0.97 ± 0.03
		Test	0.81 ± 0.10
	Formula only	Train	0.89 ± 0.02
		Test	0.74 ± 0.12
	Rheology only	Train	0.97 ± 0.03
		Test	0.82 ± 0.10
Filament roughness	Formula + rheology	Train	0.90 ± 0.03
		Test	0.78 ± 0.12
	Formula only	Train	0.84 ± 0.03
		Test	0.76 ± 0.12
	Rheology only	Train	0.88 ± 0.03
		Test	0.82 ± 0.10
Binary ink quality (Indirect prediction)	Formula + rheology	Train	0.88 ± 0.03
		Test	0.86 ± 0.11
	Formula only	Train	0.79 ± 0.04
		Test	0.78 ± 0.13
	Rheology only	Train	0.88 ± 0.04
		Test	0.87 ± 0.08
Binary ink quality (Direct prediction)	Formula + rheology	Train	0.92 ± 0.02
		Test	0.74 ± 0.13
	Formula only	Train	0.82 ± 0.03
		Test	0.70 ± 0.15
	Rheology only	Train	0.92 ± 0.02
		Test	0.75 ± 0.14

This comparison suggested that the rheological measurements formed a better feature set than the formulation parameters for ink printability prediction and adding formulation parameters to the model did not further improve the prediction accuracy. Such results were expected since the linear regression model showed that the formulation parameters were highly associated with the Rheo_PC1. Using the rheology only feature set, 0.97 and 0.82 mean accuracy was achieved for the prediction of the width label in the train and test sets respectively, and 0.88 and 0.82 for the roughness label. After a closer inspection on the misclassified samples, it was found that the most frequently misclassified samples were those predicted to print thinner and smoother filaments based on their rheological profile, but the actual prints had filaments width and roughness larger than the pre-specified thresholds (**Table S1**) used to binarize these two metrics. There was some degree of overfitting in the models for both labels. It is common for the training set to have a higher prediction accuracy than the test set. Given the small size of the test set (n = 15) in this study, even one noisy sample could reduce the accuracy of the prediction (1/15≈7%). Such variability in the test set prediction accuracy is reflected by the higher standard deviation in the repeated 5-fold cross-validation accuracy score compared to the training set (**Table 3**).

Table 4 summarized the rheological measurements of 3D food printing inks in each label class and **Figure S1** visualized their distributions stratified by the labels. Inspecting these results provided insight into the feature importance of each rheological measurement in classifying the 3D food printing ink samples with different width and roughness labels. 3D food printing inks that printed thinner filaments (width label 0) had significantly lower flow transition index, loss factor, and larger G', G", yield stress, all of which correspond to stronger gels with higher brittleness and more initial resistance to flow. On the other hand, smoother filaments (roughness label 0) often resulted from 3D food printing inks with significantly larger flow transition index, loss factor, and lower yield stress.Formulations classified as good 3D food printing inks (class 0 in the binary quality label) were the ones that achieved a balance between the two desirables but, to some extent, conflicting printing properties: thin filament width and low roughness, which made differentiating them from other formulations a challenging task. As described in Section 2.4, a direct and an indirect approach was taken to predict the binary quality label. In direct prediction, the binary quality label was directly predicted as the response using the three feature sets with cross-validation. The indirect approach combined the prediction results from the previously trained models on the width label and roughness label to obtain a predicted binary quality label in the same way as the true binary quality label was generated. As shown in **Table 3**, when using the rheological measurements as the feature set, the direct prediction approach achieved higher mean accuracy during training (0.92) compared to the indirect approach (0.88). However, it also had a higher degree of overfitting, reflected by a lower mean accuracy during testing (0.75) than the indirect approach (0.87). On the other hand, the indirect method had the same level of accuracy during training and testing, indicating limited overfitting. It could also be noticed that the mean accuracy of predicting the binary quality label with the indirect approach was higher than both the width and roughness models. The binary quality label combined the width and roughness criteria, but it sufficed to only differentiate samples with the 0-0 width-roughness combination from all other combinations. Such a scheme allowed it to absorb some prediction errors in the separate models based on width and roughness measurements and improve the prediction accuracy of the binary quality label.

Table 4. Summary of rheological measurements for 3D food printing inks (mean ± SD) stratified by width labels, roughness labels, and the width-roughness combinations

Labels	Class	Flow index	Flow transition index	Storage modulus (Pa)	Loss modulus (Pa)	Loss factor	Recovery	Yield stress (Pa)
Width	**0**	0.47 ± 0.1	2.22 ± 0.83	2475.46 ± 1857.57	230.97 ± 129.03	0.11 ± 0.03	0.79 ± 0.15	115.17 ± 101.29
	1	0.44 ± 0.12	2.87 ± 1.05	885.7 ± 1065.13	104.09 ± 142.82	0.15 ± 0.06	0.7 ± 0.16	44.39 ± 27.99
	P value[a]	0.411	0.030*	0.005*	0.005*	0.003*	0.063	0.014*
Roughness	**0**	0.44 ± 0.08	2.66 ± 0.92	1671.67 ± 1495.92	180.7 ± 132.56	0.13 ± 0.04	0.75 ± 0.14	67.56 ± 45.38
	1	0.49 ± 0.15	1.93 ± 0.8	2599.26 ± 2222.3	213.08 ± 168.99	0.1 ± 0.04	0.8 ± 0.19	144.33 ± 133.0
	P value[a]	0.116	0.011*	0.104	0.485	0.015*	0.366	0.006*
Combined	**0**	0.45 ± 0.07	2.43 ± 0.89	1954.52 ± 1515.7	203.87 ± 106.25	0.12 ± 0.03	0.76 ± 0.12	79.35 ± 47.1
	1	0.46 ± 0.13	2.41 ± 1.0	2003.92 ± 2050.1	180.67 ± 172.96	0.12 ± 0.05	0.77 ± 0.19	105.23 ± 116.93
	P value[a]	0.707	0.926	0.928	0.597	0.836	0.901	0.348

[a] The p values indicated the statistical significance of *t* test between class 0 and 1 for each rheological measurement. Significant difference ($p < 0.05$) between classes were annotated by *.

IV. DISCUSSION

A. 3D food printing inks' rheological properties are affected by AGP and AGCN concentrations, and Ca^{2+} crosslinking density

All the 3D food printing inks in the current study were formulated using different combinations of three ingredients: AGP, $CaCl_2$, and AGCN. Rheological characterization of the 3D food printing inks generated a fingerprint for each formulation. Linking the fingerprints to the formulation parameters helped unveil the structure-function relationship of the polysaccharides and ionic crosslinking in the hydrogels. Our results show that the gel strength is positively associated with AGP concentration and crosslinking density. While keeping the AGP-to-AGCN ratio constant, increasing total polysaccharides concentration from 3% to 6% resulted in a more than 10-fold increase in G' and G" at an angular frequency of 0.1 rad/s. Even with a lower crosslinking density, 6% gels were stronger than 3% gels (**Fig. 4** and **Table S3**). This result is in agreement with results reported in previous studies about AGP gelation behaviors[15, 18-21, 40, 41]. The gelation mechanism of AGP has been described using a modified "egg-box" model. Three types of AGP- Ca^{2+} complexation contribute to the gelation of AGP: rod-like junction zones between two antiparallel polyuronates chains, monocomplexes within a single polyuronates chain, and point-like crosslinking [42, 43]. In the low crosslinking density regime (R < 1) where all the 3D food printing inks formulated in the current study belong, the formation of rod-like bundles prevails and dominates over monocomplexes or point-like crosslinks [43], showing the characteristics of semiflexible polymer networks[44]. A slight increase in R in this regime allows for more extensive bundle formation among the polymer chains, resulting in a denser polymer network and a more elastic gel[41, 43, 45, 46]. Moreover, our results show that the increase in G' with R was more significant in gels with lower total polysaccharide concentration: increasing R from 0.35 to 0.55 in 3% gels led to a 10-fold increase in G', while in 6% gels, a 3-fold increase was observed (**Fig. 4**). This overall trend is attributed to the suppression of bundle

formation at higher pectin concentrations [47] in the case of AGP- Ca^{2+} gels with R < 1. Also, since only pectin can be crosslinked by calcium, not AGCN, the higher was the mass fraction of pectin in the gel, the more dominant was the crosslinking density effect on the rheological properties. Besides the linear viscoelastic characteristics, the LAOS behavior has also been used to classify complex fluids [48]. The food ink formulations in the current study all exhibited Type III LAOS behavior: at large strain amplitude, G' decreases monotonically and G" increases first then decreases (**Fig. 3**). The overshoot of G" observed in Type III fluids arises as a result of the balance between the formation and destruction of the polymer junctions under deformation [49, 50]. In the AGP- Ca^{2+} system, the structural cause of the G" overshoot is believed to be the unzipping and reformation of the egg-box bundles [47]. Eventually, at sufficiently high strain amplitude, the microstructural alignments become dominant, and both G' and G" decrease and G" exceeds G', indicating that the gel has collapsed and started to flow [49].

Another polysaccharide component in 3D food printing ink formulations was AGCN. Although previous studies have illustrated that AGCN, due to its high aspect ratio, can have outstanding mechanical properties akin to the function of cellulose in plant cell walls [15, 18-21, 31], the results of this study suggested that increasing AGCN mass fraction reduced the gel strength. This effect could be attributed to a reduction of AGP mass fraction as the total polysaccharide content was maintained constant. **Figure S2** illustrates the influence of adding AGCN to the gel while keeping the AGP concentration constant, thus increasing the total polysaccharide content. These results validate that increasing AGCN concentration significantly increases G' and G" of the gels, confirming the reinforcing effect of AGCN. However, the mass fraction of AGCN in our 3D food printing ink formulations was relatively low (at most 2.4%), and increasing AGCN concentration was always coupled with the dilution of AGP, which overshadowed the reinforcing effect of AGCN. In conclusion, the rheological characteristics of the bioinks were dominated by the AGP-calcium network, with minor contributions from the addition of AGCN.

B. Prediction of 3D food printing inks' printability from rheological characterizations

One of the key challenges in constructing a predictive model for 3D food printing inks' printability is to develop a comprehensive set of metrics for printability assessment. The two measures of printability in the current study are: smoothness of deposition and width of printed filaments. Many of the previous studies have focused on shape fidelity measurements using different methods, including measuring the width and height of the filaments [33, 51], size and circularity [23, 25] of the holes in a printed grid pattern, 'sharpness' of the angle at a corner of a printed structure [27], etc., while limited efforts have been made for quantitative characterization of smoothness of 3D food printing ink deposition. In this study, a quantitative assessment of both metrics was achieved by measuring the width and roughness of the printed filament with image analysis. In addition, 3-layer grids and 5^*5^*5 mm^3 grid cubes were printed with three representative 3D food printing ink formulations to demonstrate the stickability of the inks (**Fig. 7**). Besides establishing the quantitative metrics to assess printability, this study also constructed predictive relationships between the rheological measurements and the printability of the inks. To the best of our knowledge, among the few studies trying to relate 3D food printing inks' rheological properties to printing behaviors, only simple correlations or linear regressions have been established [6, 22]. However, both the current study and the previous studies [26, 6] have demonstrated that linear regressions are not sufficient to explain the relationship between different rheological measurements and printability metrics. Therefore, in the current study, random forest models were trained on the rheological characteristics and formulation parameters of the 3D food printing inks to predict the filament width and roughness labels and, ultimately, the binary ink quality label, combining the two metrics. However, as with many machine learning models, interpretability of the model is limited. To increase interpretability, this study analyzed the difference between 3D food printing inks from different width and roughness groups. And the results showed that none of the rheological measurements were significantly different between the two binary quality classes (**Table 4**). This was expected since the "non-optimal" 3D food printing inks group (class 1 in the binary quality label) included the ones that were either too weak or too strong to be printed, resulting in a wide range of rheological properties within this group. Therefore, direct prediction of ink quality could be challenging. An alternative indirect approach trained two separate models on the width and roughness labels and combined the classification results from both models to generate the predicted binary quality label. Comparing the prediction results using the direct and indirect approaches, it could be concluded that the indirect method achieved higher mean accuracy and less overfitting. Given the relatively small sample size, especially with a nonlinear relationship, the direct prediction models were more susceptible to outliers and overfitting. With an increase in the sample size, the model performance was expected to improve further. Another advantage of using the indirect prediction approach was that the width and roughness model provided guidance on downstream improvement of the 3D food printing ink based on the predicted limitation of the printability metrics. Different feature sets were also compared for their prediction capacity: formulation parameters, rheological measurements, and combined. Models trained with rheological measurements alone showed the best

prediction accuracy among the three feature sets, implicating that it is possible to generalize the model beyond the current formulation parameters to other polysaccharide-based compositions. The evidence from this and other studies[17, 24, 32] supported that rheological fingerprints of hydrogel-based 3D food printinginks are often well correlated with the formulation parameters, but their relationship with printability is complicated and nonlinear. Rheological characterization is versatile for hydrogels formulated with different compositions. For future 3D food printing ink development with potentially different ingredients, models trained using formulation parameters would not be applicable, but those trained with rheological measurements could still be valid. A more robust dataset including rheological measurements of inks with other compositions should be constructed to achieve better generalizability of the model.

V. CONCLUSION

All the 3DHydrogel-based food inks formulated with low methoxy pectin, cellulose nanocrystals and calcium chloride were developed, characterized, and successfully 3D printed. Calcium-crosslinked AGP hydrogel maintained the 3D network of the food inks, and AGCN exhibited a micro enforcing effect akin to their functionality in plant cell walls. The rheological properties of the hydrogels were found to be linearly associated with the formulation parameters. Printability of the 3D food printing inks was assessed and quantified with two metrics: printed filaments' width and roughness. The ink printability could be predicted with high accuracy with random forest classifiers trained on the rheological measurements without specifying formulation parameters, demonstrating the possibility to generalize the model to 3D food printing inks with different compositionsin food manufacturing processes such as alternative foods and nanofoods.

ACKNOWLEDGEMENT

REFERENCES

[1]. A. Derossi, R. Caporizzi, D. Azzollini and C. Severini, "Application of 3D printing for customized food. A case on the development of a fruit-based snack for children," Journal of Food Engineering, vol 220, pp.65–75, 2018.

[2]. M. Askari, M. Afzali Naniz, M. Kouhi, A. Saberi, A. Zolfagharian and M. Bodaghi, "Recent progress in extrusion 3D bioprinting of hydrogel biomaterials for tissue regeneration: A comprehensive review with focus on advanced fabrication techniques," Biomaterials Science, vol. 9, no. 3, pp. 535–573, 2021.

[3]. J. Sun, W. Zhou, L. Yan, D. Huang and L. Lin, "Extrusion-based food printing for digitalized food design and nutrition control," Journal of Food Engineering, vol. 220, pp. 1–11, 2017.

[4]. L. Hao, S.Mellor, O. Seaman, J. Henderson, N. Sewell and M. Sloan, "Material characterizationand process development for chocolate additive layer manufacturing," Virtual and Physical Prototyping, vol. 5, no. 2, pp. 57–64, 2010.

[5]. C. Severini, A. Derossi and D. Azzollini, "Variables affecting the printability of foods: Preliminary tests on cereal-based products," Innovative Food Science & Emerging Technologies, vol. 38, pp. 281–291, 2016.

[6]. S. Zhu, M. A. Stieger, A. J. van der Goot and M. A. I. Schutyser, "Extrusion-based 3D printing of food pastes: Correlating rheological properties with printing behavior," Innovative Food Science & Emerging Technologies, vol. 58, pp. 102-214, 2019.

[7]. D. L. Cohen, J. I. Lipton, M. Cutler, D. Coulter, A. Vesco and H. Lipson, "Hydrocolloid printing: a novel platform for customized food production. University of Hydrocolloid Printing: A Novel Platform for Customized Food Production," Cornell University, 2009.

[8]. R. Serizawa, M. Shitara, J. Gong, M. Makino, M. H. Kabir andH. Furukawa, "3D jet printer of edible gels for food creation," In N. C. Goulbourne & H. E. Naguib (Eds.), Behavior and Mechanics of Multifunctional Materials and Composites,vol. pp. 9058-9069,2014.

[9]. H. Ismail, M. Irani, andZ. Ahmad, "Starch-based hydrogels: Present status and applications," International Journal of Polymeric Materials and Polymeric Biomaterials, vol. 62, no. 7, pp. 411–420, 2014.

[10]. T. Agarwal, M. Costantini and T. K. Maiti, "Extrusion 3D printing with Pectin-based ink formulations: Recent trends in tissue engineering and food manufacturing," Biomedical Engineering Advances, vol. 2, pp. 100018, 2021.

[11]. R. S. M. Azam, M. Zhang, B. Bhandari and C. Yang, "Effect of different gums on features of 3D printed object based on vitamin-D enriched orange concentrate," Food Biophysics, vol. 13, no. 3, pp. 250–262, 2018.

[12]. K. Markstedt, A. Mantas, I. Tournier, H. Martínez Avila, D. Hagg and P. Gatenholm, "3D bioprinting human chondrocytes with nanocellulose-alginate bioink for cartilage tissue engineering applications," Biomacromolecules, vol. 16, no. 5, pp. 1489–1496, 2015.

[13]. V. Vancauwenberghe, P. Verboven, J. Lammertyn and B. Nicolaï, "Development of a coaxial extrusion deposition for 3D printing of customizable pectin-based food simulant," Journal of Food Engineering, vol. 225, pp. 42–52,2018.

[14]. O. Yildirim and A.Arslan-Yildiz, "Development of a hydrocolloid bio-ink for 3D bioprinting," Biomaterials Science, vol. 10, no. 23, pp. 6707–6717,2022.

[15]. D. M. Kim and H. S. Kwak, "Development of functional nanofood and its future," J. Kor. Dairy Technol. Sci., vol. 23, no. 1, pp. 19-26, 2005.

[16]. D. M. Kim, E. C. Cha and K. J. Chung, "Pharmacognosy for medical nanofood in the 21st century," J. Food Sci. Nutr., vol. 10, pp. 95-102, 2005.

[17]. X. Zeng, H. Chen, L. Chen and B. Zheng, "Insights into the relationship between structure and rheological properties of starch gels in hot-extrusion 3D printing," Food Chemistry, vol. 342, pp. 128362, 2021.

[18]. D. M. Kim, "Various types and manufacturing techniques of nano and micro capsules for nanofood," J. Kor. Dairy Sci. Technol., vol. 24, no. 1, pp. 53-63, 2006.

[19]. D. M. Kim and G. D. Lee, "Introduction to the technology, applications, products, Markets R&D, and perspectives of nanofoods in the food industry," J. Food Sci. Nutr., vol. 11, pp. 348-357, 2006.

[20]. D. M. Kim and G. S. Cho, "Nanofood and its materials as Nutrient Delivery System (NDS)," Agric. Chem. Biotechnol., vol. 49, no. 2, pp. 39-47, 2006.

[21]. D. M. Kim, "Preparation of smart probiotic solid lipid nanoparticles (SLN) for target controlled nanofood," J. Kor. Dairy Sci. Technol., vol. 25, no. 2, pp. 5-10, 2007.

[22]. X. Zeng, T. Li, J. Zhu, L. Chen and B. Zheng, "Printability improvement of rice starch gel via catechin and procyanidin in hot extrusion 3D printing," Food Hydrocolloids, vol. 121, pp. 106997-107003,2021.

[23]. S. Kyle, Z.M. Jessop, A. Al-Sabah and Whitaker, I. S. (2017). "Printability" of Candidate Biomaterials for Extrusion Based 3D Printing: State-of-the-Art. Advanced Healthcare Materials, vol. 6, no. 16, pp. 231-239,2017.

[24]. Z. Liu, H. Chen, B. Zheng, F. Xie and L. Chen, "Understanding the structure and rheological properties of potato starch induced by hot-extrusion 3D printing," Food Hydrocolloids, vol. 105, pp. 105812-105821, 2020

[25]. L. Ouyang, R. Yao, Y. Zhao and W. Sun, "Effect of bioink properties on printability and cell viability for 3D bioplotting of embryonic stem cells," Biofabrication, vol. 8, no. 3, pp. 35020-35031,2016.

[26]. Z. Liu, B. Bhandari, S. Prakash, S. Mantihal and M. Zhang, "Linking rheology and printability of a multicomponent gel system of carrageenan-xanthan-starch in extrusion based additive manufacturing," Food Hydrocolloids, vol. 87, pp. 413–424,2019.

[27]. Y. He, F. Yang, H. Zhao, Q. Gao, B. Xia and J. Fu, "Research on the printability of hydrogels in 3D bioprinting," Scientific Reports, vol. 6, pp. 29977-29989,2016.

[28]. Y. Ma, M. A. I. Schutyser, R. M. Boom andL. Zhang, "Predicting the extrudability of complex food materials during 3D printing based on image analysis and gray-box data-driven modelling," Innovative Food Science & Emerging Technologies, vol. 73, 102764-102778,2021.

[29]. P. Lopez-Sanchez, M. Martinez-Sanz, M. R. Bonilla, D. Wang, E. P. Gilbert, J. R. Stokes and M. J. Gidley, "Cellulose-pectin composite hydrogels: Intermolecular interactions and material properties depend on order of assembly," Carbohydrate Polymers, vol. 162, pp. 71–81, 2017.

[30]. M. K. Hausmann, P. A. Rühs, G. Siqueira, J. Lauger, R. Libanori, T. Zimmermann and A. R. Studart, "Dynamics of cellulose nanocrystal alignment during 3D printing," ACS Nano, vol. 12, no. 7, pp. 6926–6937, 2018.

[31]. G. Siqueira, D. Kokkinis, R. Libanori, M. K. Hausmann, A. S. Gladman, A. Neels and A. R. Studart, "Cellulose nanocrystal inks for 3D printing of textured cellular architectures," Advanced Functional Materials, vol. 27, no. 12, pp. 1604619-164628, 2017.

[32]. V. Vancauwenberghe, L. Katalagarianakis, Z. Wang, M. Meerts, M. Hertog, P. Verboven and B.Nicolaï, "Pectin based food-ink formulations for 3-D printing of customizable porous food simulants," Innovative Food Science & Emerging Technologies, vol. 42, pp. 138–150, 2017.

[33]. A. Conev, E. E. Litsa, M. R. Perez, M. Diba, A. G. Mikos and L. E. Kavraki, "Machine AI learningguided three-dimensional printing of tissue engineering scaffolds," Tissue Engineering. Part A, vol. 26, no. 23–24, pp. 1359–1368,2020.

[34]. C. C. Hung and P. H. Santschi, P. H. "Spectrophotometric determination of total uronic acids in seawater using cation-exchange separation and pre-concentration by lyophilization," Analytica Chimica Acta, vol. 427, no. 1, pp. 111–117,2001.

[35]. J. Müller-Maatsch, M. Bencivenni, A. Caligiani, T. Tedeschi, G. Bruggeman, M. Bosch and S. Sforza, "Pectin content and composition from different food waste streams," Food Chemistry, vol. 201, pp. 37–45, 2016.

[36]. H. Li, Y. J. Tan, K. F. Leong andL. Li, "3D Bioprinting of highly thixotropic alginate/methylcellulose hydrogel with strong interface bonding,' ACS Applied Materials & Interfaces, vol. 9, no. 23, 20086–20097,2017.

[37]. M.Dabbaghi, S. Namjoshi, B. Panchal, J. E. Grice, S. Prakash, M. S. Roberts and Y. Mohammed, "Viscoelastic and deformation characteristics of structurally different commercial topical systems," Pharmaceutics, vol. 13, no. 9, pp. 232-242,2021.

[38]. G. Stojkov, Z. Niyazov, F. Picchioni and R. K. Bose, "Relationship between structure and rheology of hydrogels for various applications, Gels, vol. 7, no. 4,pp. 372-383, 2021.

[39]. M. A. Rao, "Measurement of flow and viscoelastic properties:" In rheology of fluid, semisolid, and solid foods,"Springer US,pp. 63–159,2014.

[40]. S. M. Cardoso, M. A. Coimbra andJ. A. Lopes da Silva, "Calcium-mediated gelation of an olive pomace pectic extract," Carbohydrate Polymers, vol. 52, no. 2, pp. 125–133,2003.

[41]. I. Fraeye, E. Doungla, T. Duvetter, P. Moldenaers, A. Van Loey and M. Hendrickx, "Influence of intrinsic and extrinsic factors on rheology of pectin–calcium gels," Food Hydrocolloids, vol. 23, no. 8,pp. 2069–2077,2009.

[42]. L.Cao, W. Lu, A. Mata, K. Nishinari and Y. Fang, "Egg-box model-based gelation of alginate and pectin: A review," Carbohydrate Polymers, vol. 242, pp. 116389-116398,2020.

[43]. I. Ventura, J. Jammal and H. Bianco-Peled, "Insights into the nanostructure of low-methoxyl pectin-calcium gels," Carbohydrate Polymers, vol. 97, no. 2, pp. 650–658,2013.

[44]. R. R. Vincent and M. A. K. Williams, "Microrheological investigations give insights into the microstructure and functionality of pectin gels," Carbohydrate Research, vol. 344, no. 14, pp. 1863–1871,2009.

[45]. A. Cardenas, F. M. Goycoolea andM. Rinaudo, "On the gelling behaviour of 'nopal' (Opuntia ficus indica) low methoxyl pectin," Carbohydrate Polymers, vol. 73, no. 2, pp. 212–222,2008.

[46]. D. Lootens, F. Capel, D. Durand, T. Nicolai, P. Boulenguer and V. Langendorff, "Influence of pH, Ca concentration, temperature and amidation on the gelation of low methoxyl pectin," Food Hydrocolloids, vol. 17, no. 3, pp. 237–244,2003.

[47]. J. John, D. Ray, V. K. Aswal, A. P. Deshpande and S. Varughese, "Dissipation and strain-stiffening behavior of pectin-Ca gels under LAOS," Soft Matter, vol. 15, no. 34, pp. 6852–6866, 2019.

[48]. K. Hyun, S. H. Kim, K. H. Ahn and S. J. Lee, "Large amplitude oscillatory shear as a way to classify the complex fluids," Journal of Non-Newtonian Fluid Mechanics, vol. 107, no. 1–3), pp. 51–65, 2002.

[49]. K. Hyun, M. Wilhelm, C. O. Klein, K. S. Cho, J. G. Nam, K. H. Ahn and G. H. McKinley, "A review of nonlinear oscillatory shear tests: Analysis and application of large amplitude oscillatory shear (LAOS)," Progress in Polymer Science, vol. 36, no. 12, pp. 1697–1753,2011.

[50]. H. G. Sim, K. H. Ahn and S. J. Lee, "Large amplitude oscillatory shear behavior of complex fluids investigated by a network model: A guideline for classification," Journal of Non-Newtonian Fluid Mechanics, vol. 112, no. 2–3, pp. 237–250,2003.

[51]. X. Zeng, H. Chen, L. Chen and B. Zheng, "Insights into the relationship between structure and rheological properties of starch gels in hot-extrusion 3D printing," Food Chemistry, vol. 342, pp. 128362-128377, 2021.